LA-UR- 09-06917

Approved for public release;
distribution is unlimited.

Title:	Plasticity Microstructure Characteristics using 3D Voronoi Structures
Author(s):	Ben Hansen-T-3 Curt Bronkhorst-T-3
Intended for:	Materials Science & Technology Meeting Pittsburg, PA USA October 25-29, 2009

Los Alamos
NATIONAL LABORATORY
EST. 1943

Form 836 (7/06)

Plasticity Microstructure Characteristics using 3D Voronoi Structures

BL Hansen, CA Bronkhorst

Theoretical Division, Los Alamos National Laboratory, Los Alamos, NM

First a comparison is made between direct single crystal simulations run on 3D Voronoi single crystal structures analyzing the need to run simulations with 3D microstructures. The simulations are preformed to large deformations at high strain rates using traditional plasticity models with the finite element method. Voronoi tessellations are used due to the ability to apply finite element meshes to such structures. The concerns of meshing these structures and successful techniques will be discussed. Laminate models of dislocation structures are considered to include size effects of the crystals for future simulations.

Plasticity Microstructure Characteristics using 3D Voronoi Structures

Benjamin L. Hansen, Curt A. Bronkhorst

Theoretical Division
Los Alamos National Laboratory

LA-UR 09-????

Los Alamos NATIONAL LABORATORY EST. 1943

Motivation

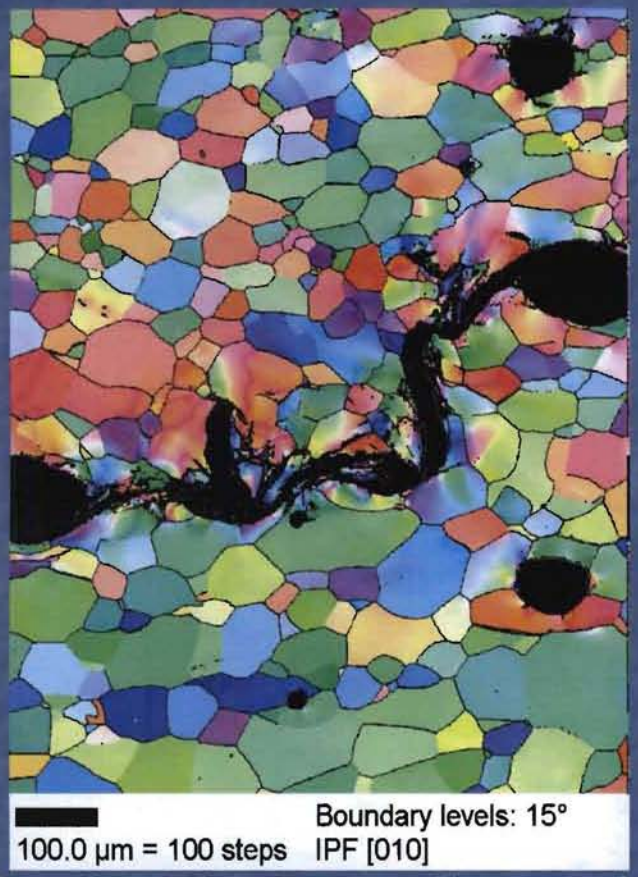

Tantalum Plate Impact Compression
OIM: B. Henrie, MST-8, LANL

- Microstructure properties effect continuum material response.
- Material damage (e.g. intergranular corrosion cracking, void nucleation) and high deformation mechanisms (eg. shear banding) are local.
- Localizations occur because of inhomogeneities in the material.
- The innate inhomogeneities of metallic materials are caused by the underlying polycrystalline microstructure.

- Goal is to simulate statistically equivalent polycrystalline microstructures. Validate to experimental measurements.

Cu Plane Strain Compression

Undeformed $\varepsilon = -1.5$

Voronoi

- Voronoi cells used as approximation of grain structure.
- Voronoi cells are based off an idealized grain growth model - provide a good approximation.
- Convex cells.
- Fewer complications in meshing.
- Currently using PyXL software from Cornel Fracture Group
- Length scale appropriate simulation involves
  - Individual distinguished grains
  - Material model accounts for deformation (including hardening and texture characteristics of grain).

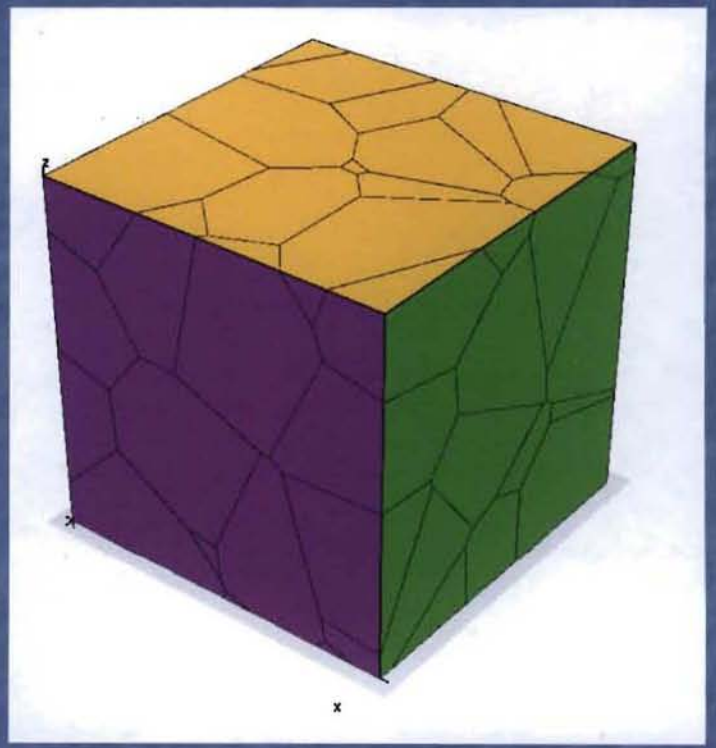

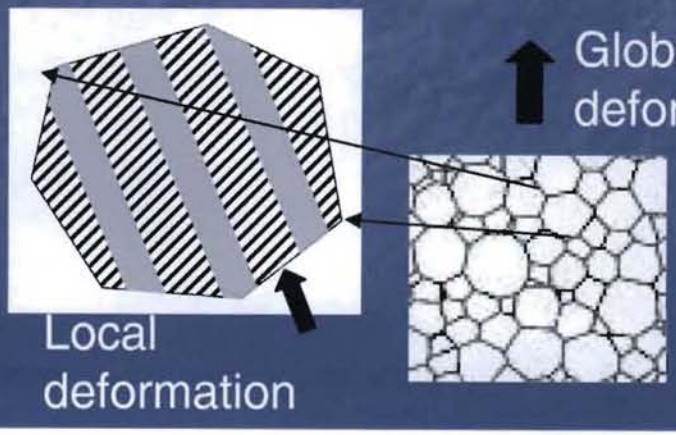

Single crystal model

Asaro & Rice (1977) , Acharya & Beaudoin (2000),
Kothari & Anand (1998), Busso et al. (2000), Kocks (1976)
Kalidindi et al. (1992), Bronkhorst et al. (1992), Anand (1998)

Stress

$$\mathbf{T}^* = \mathbf{L}\left[\mathbf{E}^* - \mathbf{A}(\theta - \theta_0)\right]$$

$$\mathbf{E}^* \equiv \frac{1}{2}\left(\mathbf{F}^{*T}\mathbf{F}^* - \mathbf{1}\right)$$

$$\mathbf{T}^* \equiv \mathbf{F}^{*-1}\left(\det \mathbf{F}^*\right)\mathbf{T}\mathbf{F}^{*-T}$$

$$\mathbf{F}^* = \mathbf{F}\mathbf{F}^{p^{-1}}$$

Hardening

$$\dot{s}^\alpha = \sum_\beta h^{\alpha\beta}\left|\dot{\gamma}^\beta\right| \qquad h^{\alpha\beta} = \left[r + (1-r)\,\delta^{\alpha\beta}\right]h^\beta$$

$$h^\beta = h_o\left(\frac{s_s^\beta - s^\beta}{s_s^\beta - s_0^\beta}\right)$$

$$s_s^\beta = \hat{s}_s^\beta(\dot{\gamma}, \theta) = s_{s_0}\left(\frac{\dot{\gamma}^\beta}{\dot{\gamma}_0}\right)^{\frac{k\theta}{A}}$$

Flow Rule

$$\mathbf{L}^p = \dot{\mathbf{F}}^p\mathbf{F}^{p^{-1}} = \sum_\alpha \dot{\gamma}^p \mathbf{S}_0^\alpha \qquad \mathbf{S}_0^\alpha \equiv \mathbf{m}_0^\alpha \otimes \mathbf{n}_0^\alpha$$

$$\dot{\gamma}^\alpha = \dot{\gamma}_0 \exp\left[-\frac{F_0}{k\theta}\left\langle 1 - \left\langle \frac{\left|\tau^\alpha\right| - s^\alpha \dfrac{\mu}{\mu_0}}{s_1^\alpha \dfrac{\mu}{\mu_0}} \right\rangle^p \right\rangle^q\right]\operatorname{sgn}\left(\tau^\alpha\right)$$

$$\tau^\alpha \equiv \left(\mathbf{C}^*\mathbf{T}^*\right)\cdot\mathbf{S}_0^\alpha$$

$$\mathbf{C}^* = \mathbf{F}^{*T}\mathbf{F}^*$$

$$\frac{\mu}{\mu_0} \equiv \frac{C_{12}}{C_{12_0}} = 1 + \frac{m_{12}}{C_{12_0}}\theta$$

Simmons & Wang, 1971

Texture

$$\mathbf{m}^\alpha = \mathbf{F}^*\mathbf{m}_0^\alpha$$

$$\mathbf{n}^\alpha = \mathbf{F}^{*-T}\mathbf{n}_0^\alpha$$

Adiabatic Heating

$$\dot{\theta} = \frac{\eta}{\rho c_p}\sum_\alpha \tau^\alpha \dot{\gamma}^\alpha$$

Material Parameter Evaluation

Parameters:

$\rho = 16640$ kg/m^3	$r = 1.4$
$c_p = 150$ J/kg-K	$\dot{\gamma}_0 = 10^7$ sec^{-1}
$\alpha = 6.5$ μm/m-K	$s_0 = 50$ MPa
$\eta = 0.0, 0.95$	$s_l = 550$ MPa
$m_{11} = -24.5$ MPa/K	$F_0 = 2.1\times10^{-19}$ J
$C_{11_0} = 268.5$ GPa	$p = 0.34$
$m_{12} = -11.8$ MPa/K	$q = 1.66$
$C_{12_0} = 159.9$ GPa	$s_{s_0} = 125$ MPa
$m_{44} = -14.9$ MPa/K	$h_{s_0} = 300$ MPa
$C_{44_0} = 87.1$ GPa	$A = 10^{-18}$ J

Ta - 24 BCC systems
{110}<111> , {112}<111>

Cu - 12 FCC systems
{111}<110>

Material Parameter Evaluation
512 Elements/Grains

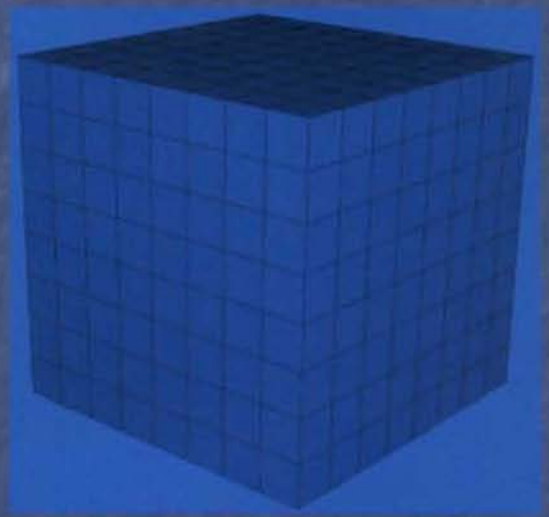

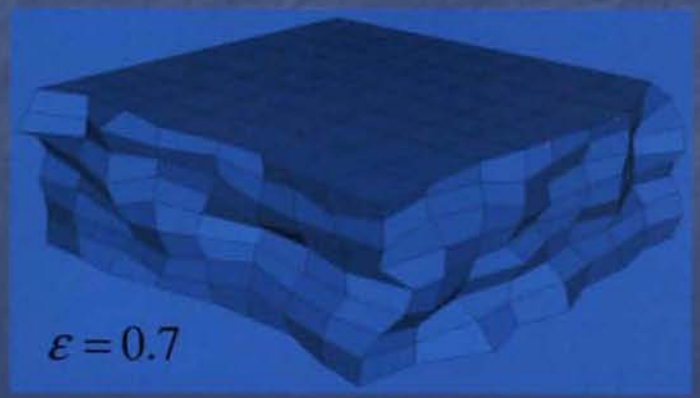

Single crystal model - Ta

Initial Texture

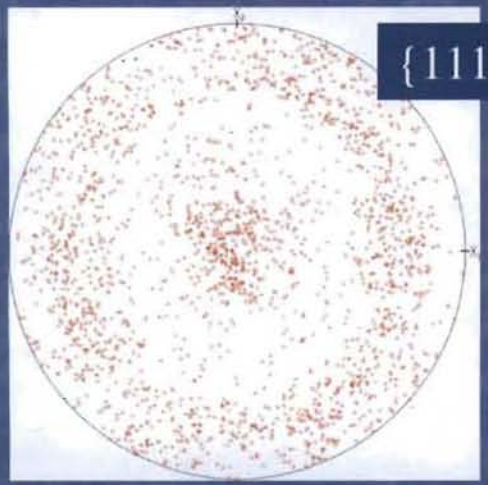

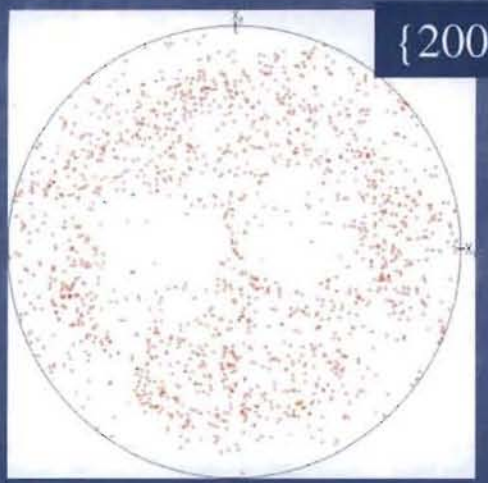

$\rho = 16640$ kg/m^3
$c_p = 150$ J/kg-K
$\alpha = 6.5$ μm/m-K
$\eta = 0.0.0.95$
$m_{11} = -24.5$ MPa/K
$C_{11_0} = 268.5$ GPa
$m_{12} = -11.8$ MPa/K
$C_{12_0} = 159.9$ GPa
$m_{44} = -14.9$ MPa/K
$C_{44_0} = 87.1$ GPa
$r = 1.4$

$\dot{\gamma}_0 = 10^7$ sec^{-1}
$s_0 = 50$ MPa
$s_i = 550$ MPa
$F_0 = 2.1\times10^{-19}$ J
$p = 0.34$
$q = 1.66$
$s_{s_0} = 125$ MPa
$h_{s_0} = 300$ MPa
$A = 10^{-18}$ J

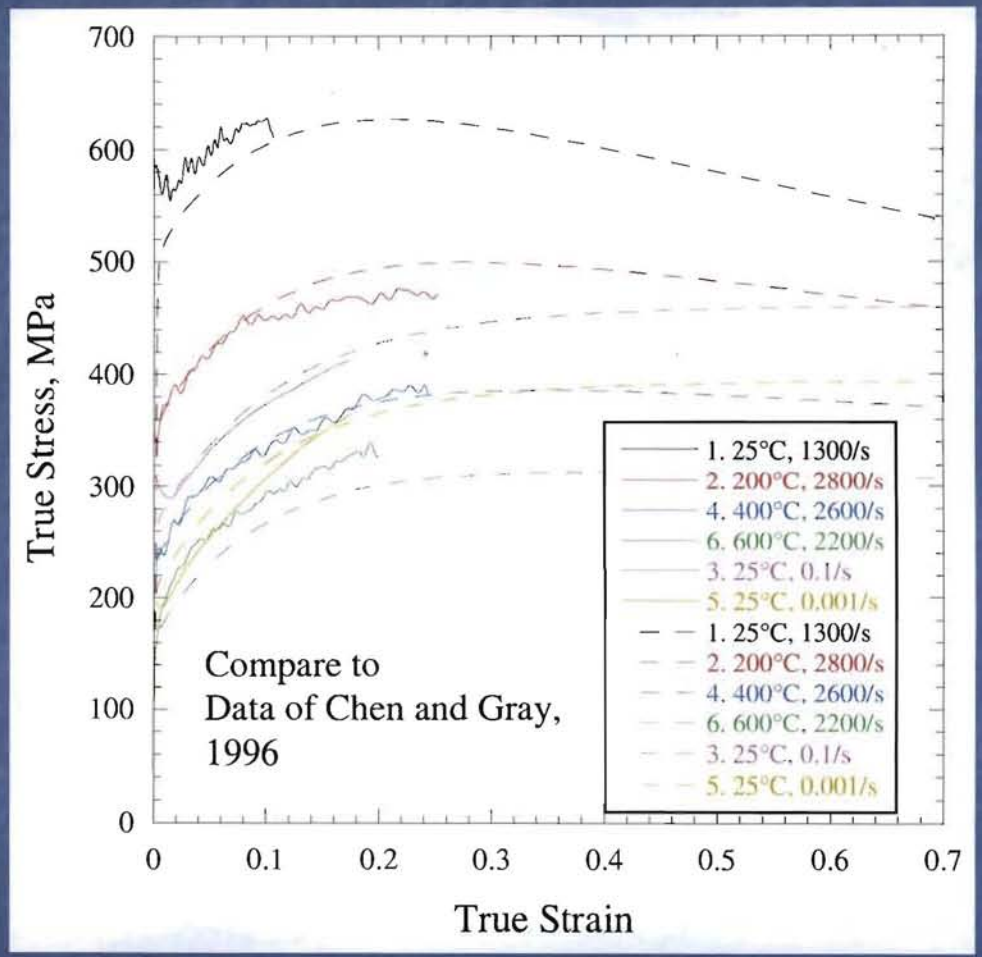

Single crystal model - Cu

$\rho = 8960$ kg/m^3
$c_p = 380$ J/kg-K
$\alpha = 17.7$ μm/m-K
$\eta = 0.0, 0.95$
$m_{11} = -36.3$ MPa/K
$C_{11_0} = 179.5$ GPa
$m_{12} = -16.4$ MPa/K
$C_{12_0} = 126.4$ GPa
$m_{44} = -25.7$ MPa/K
$C_{44_0} = 82.5$ GPa
$r = 1.4$

$\dot{\gamma}_0 = 10^7$ sec^{-1}
$s_0 = 1$ MPa
$s_i = 20$ MPa
$F_0 = 1.0\times10^{-18}$ J
$p = 0.33$
$q = 1.66$
$s_{s_0} = 205$ MPa
$h_{s_0} = 200$ MPa
$A = 1.5\times10^{-19}$ J

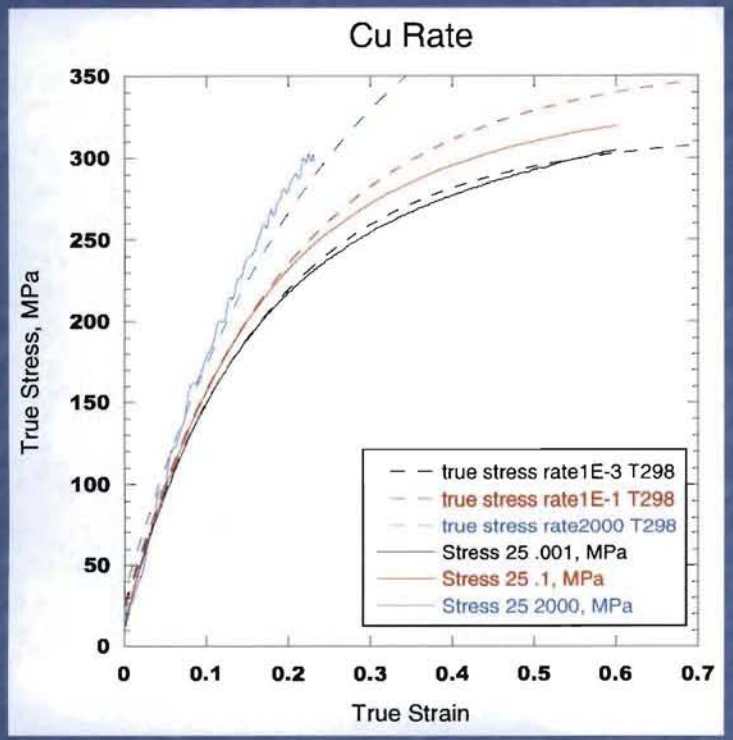

Initial Texture: Random

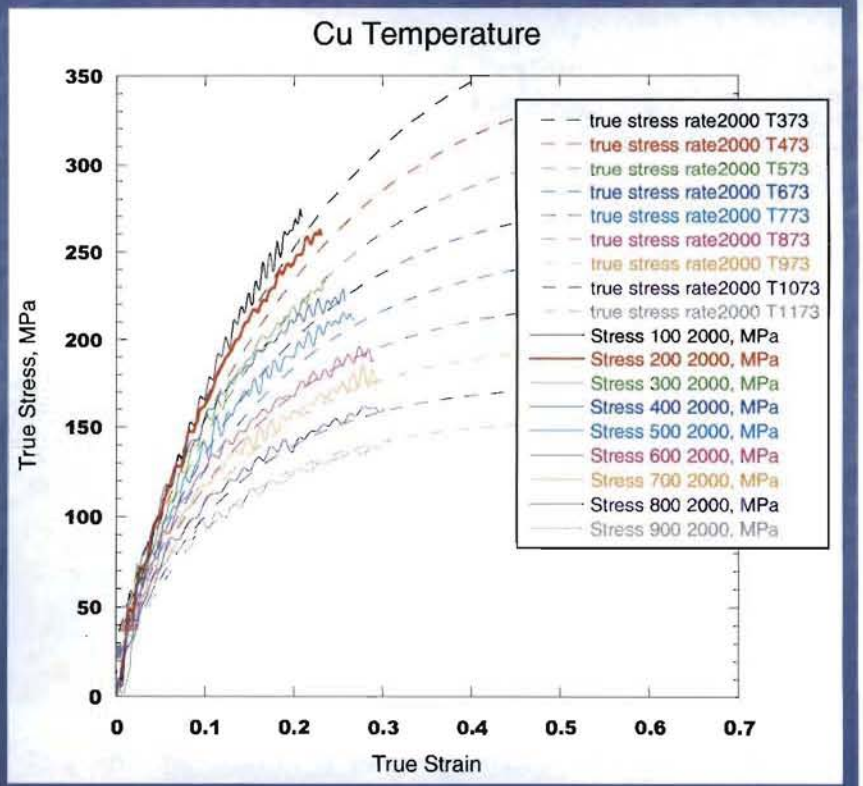

Tetgen Meshes

- Looking for Delaunay mesh generation for convex shapes.
- Generates tetrahedral meshes in 3D with internal faces respected.
- Not all slivers always removed.
- Quality of meshes is sufficient to run simulations.
- Meshing is a difficult prospect due to the constraint placed on meshing by the intersection of grain faces.

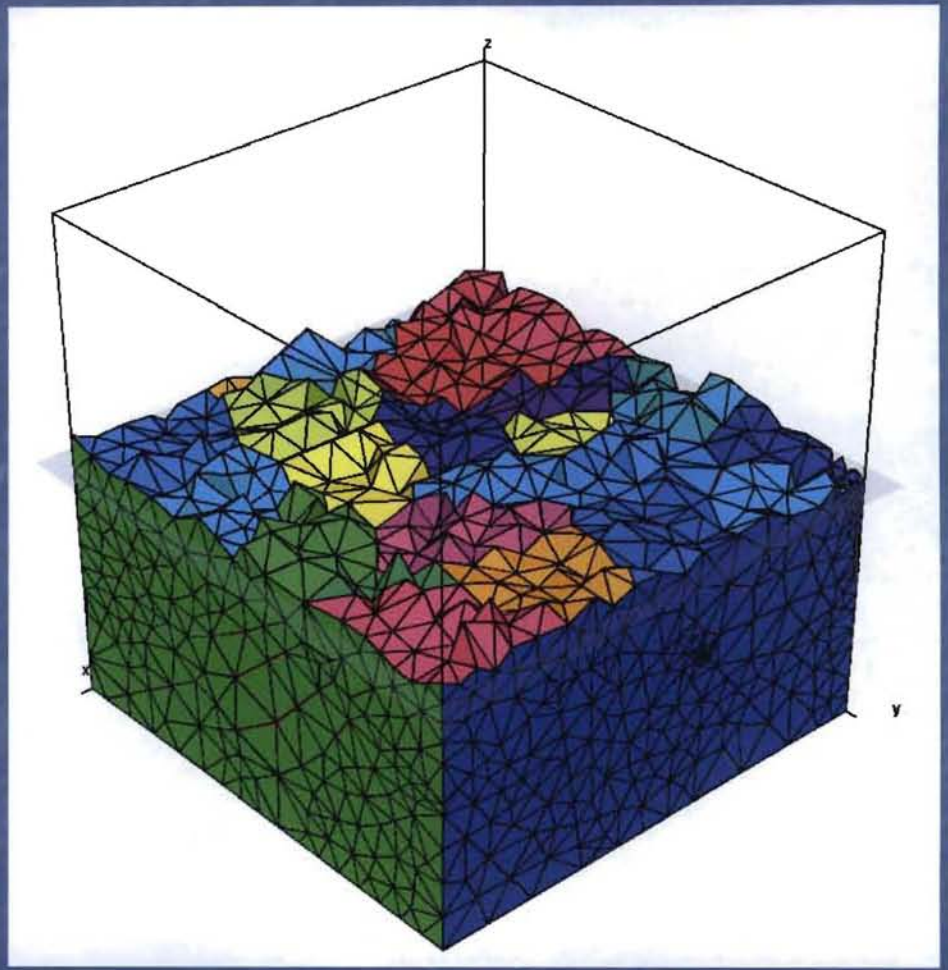

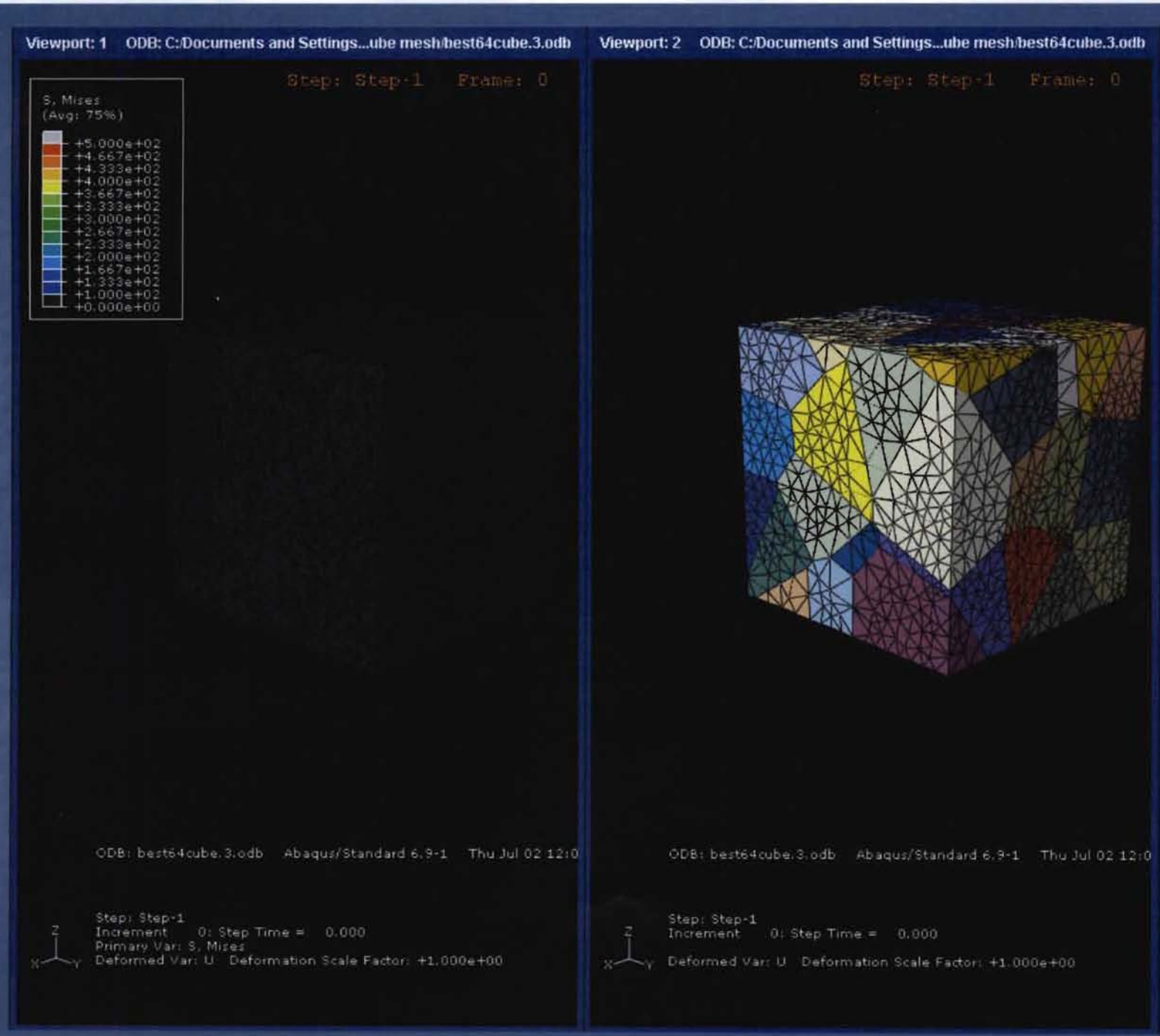
Viewport: 1 ODB: C:/Documents and Settings...ube mesh/best64cube.3.odb
Step: Step-1 Frame: 0
S, Mises
(Avg: 75%)
+5.000e+02
+4.667e+02
+4.333e+02
+4.000e+02
+3.667e+02
+3.333e+02
+3.000e+02
+2.667e+02
+2.333e+02
+2.000e+02
+1.667e+02
+1.333e+02
+1.000e+02
+0.000e+00
ODB: best64cube.3.odb Abaqus/Standard 6.9-1 Thu Jul 02 12:0
Step: Step-1
Increment 0: Step Time = 0.000
Primary Var: S, Mises
Deformed Var: U Deformation Scale Factor: +1.000e+00
Viewport: 2 ODB: C:/Documents and Settings...ube mesh/best64cube.3.odb
Step: Step-1 Frame: 0
ODB: best64cube.3.odb Abaqus/Standard 6.9-1 Thu Jul 02 12:0
Step: Step-1
Increment 0: Step Time = 0.000
Deformed Var: U Deformation Scale Factor: +1.000e+00

Individual Grains

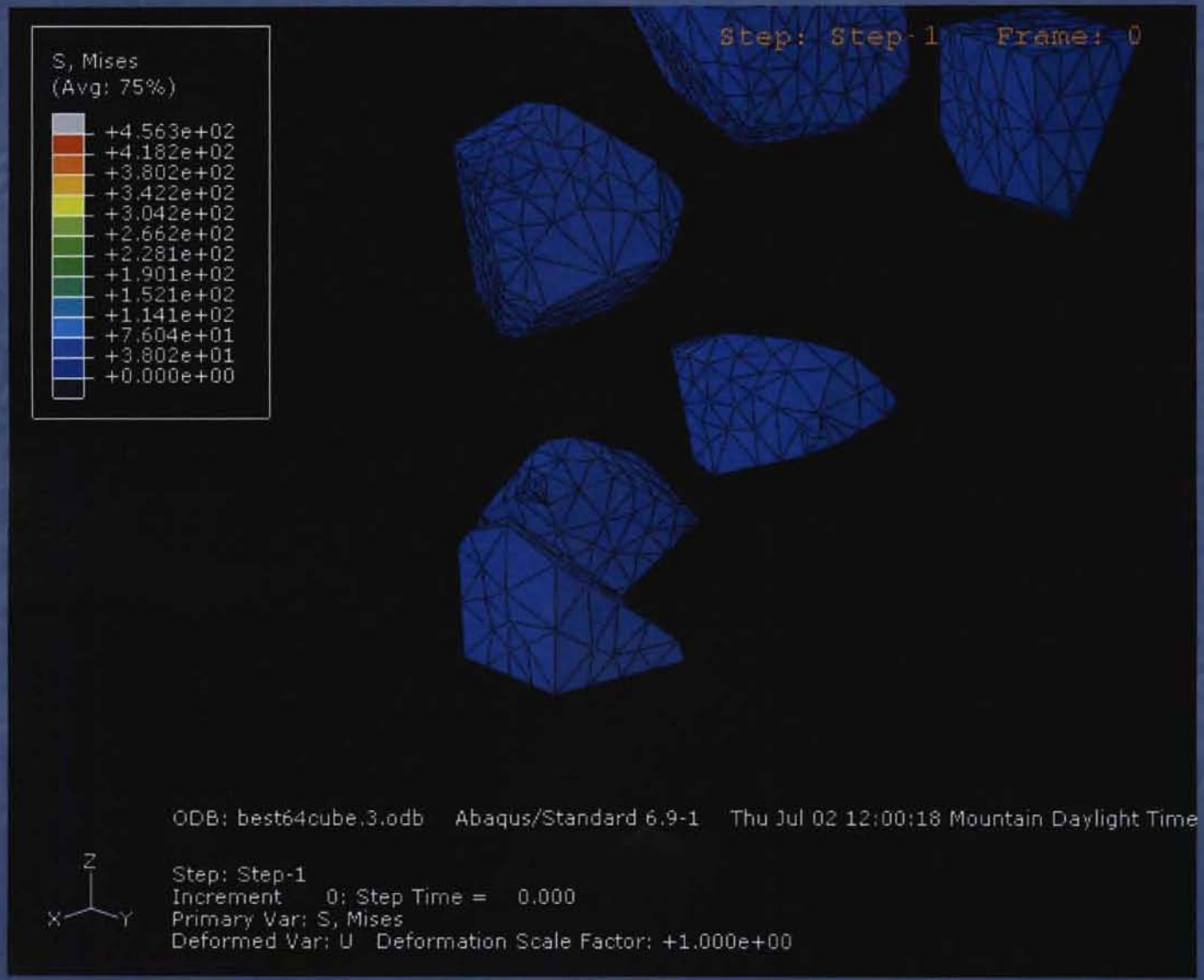

Mesh Sensitivity

64 grains

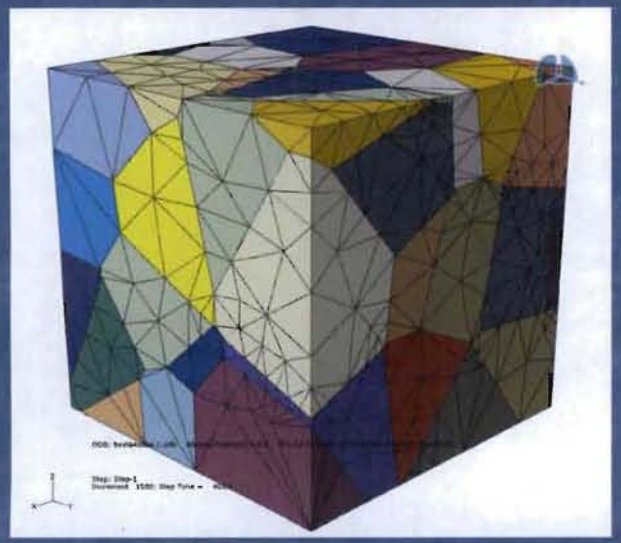

11175 Tet. Elements

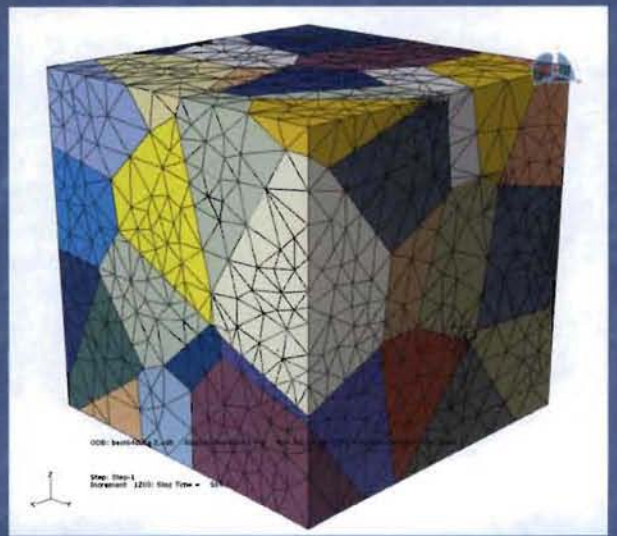

23544 Tet. Elements

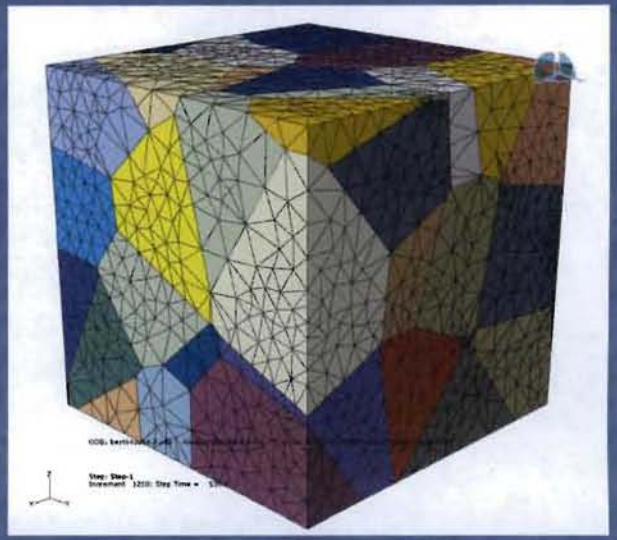

43141 Tet. Elements

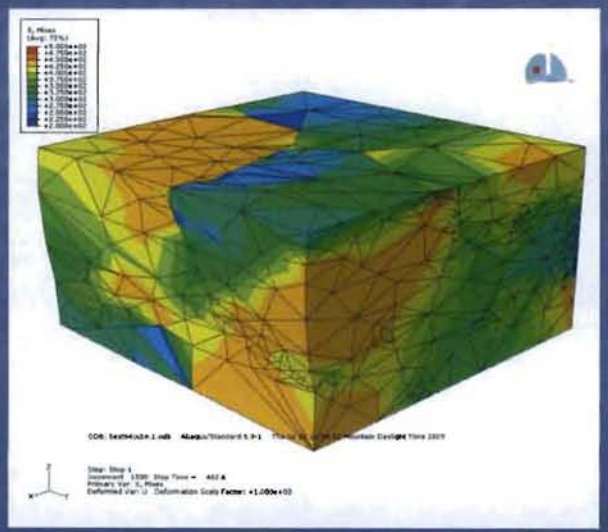

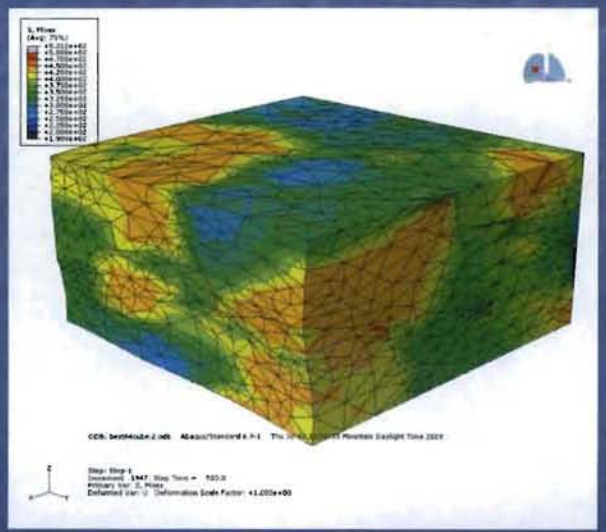

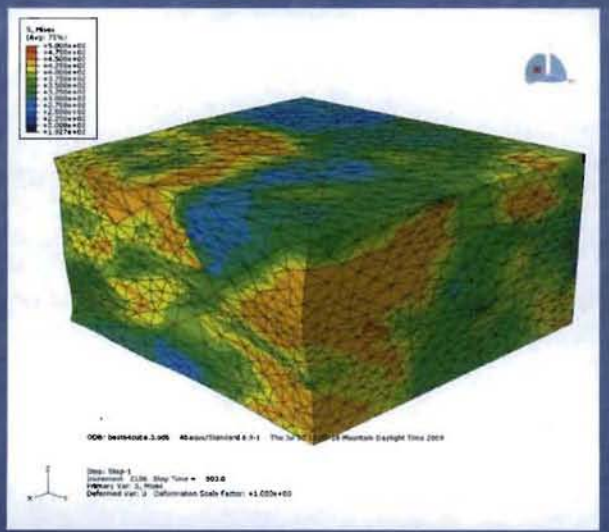

Crystallographic Texture

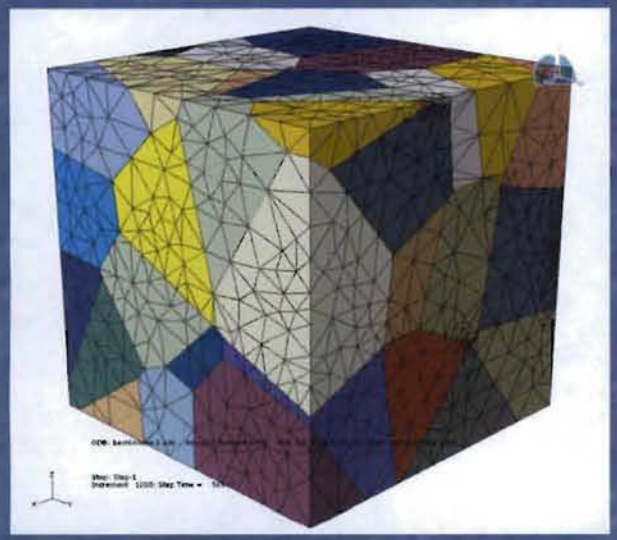

23544 Tet. Elements

64 grains

3 sets of 64 random crystal orientations

Texture 1:

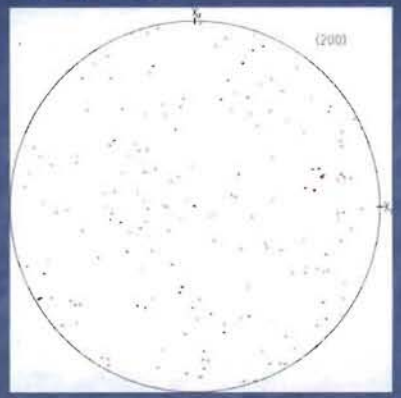

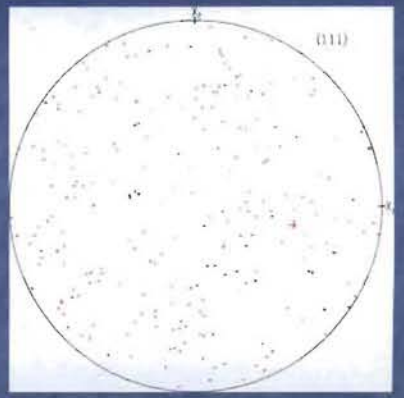

Texture 2:

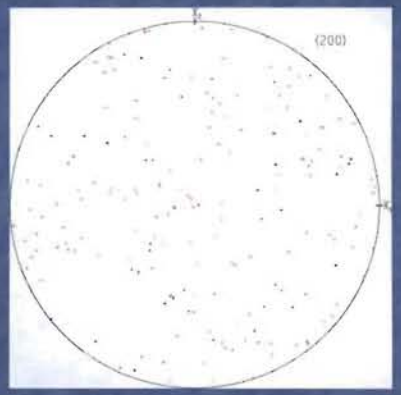

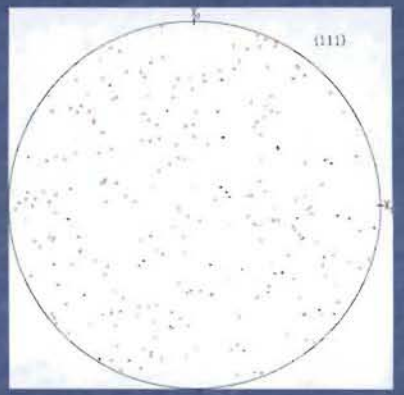

Texture 3:

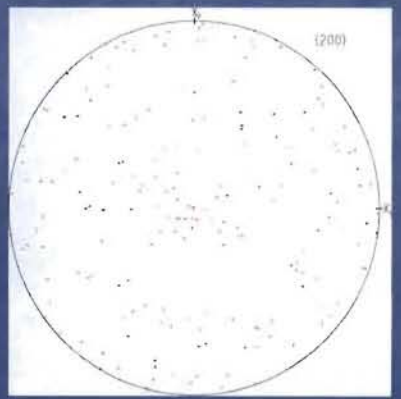

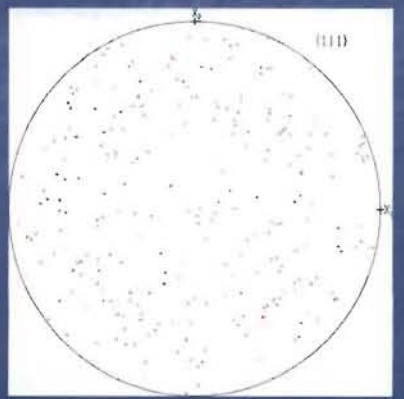

Crystallographic Response

Texture 1

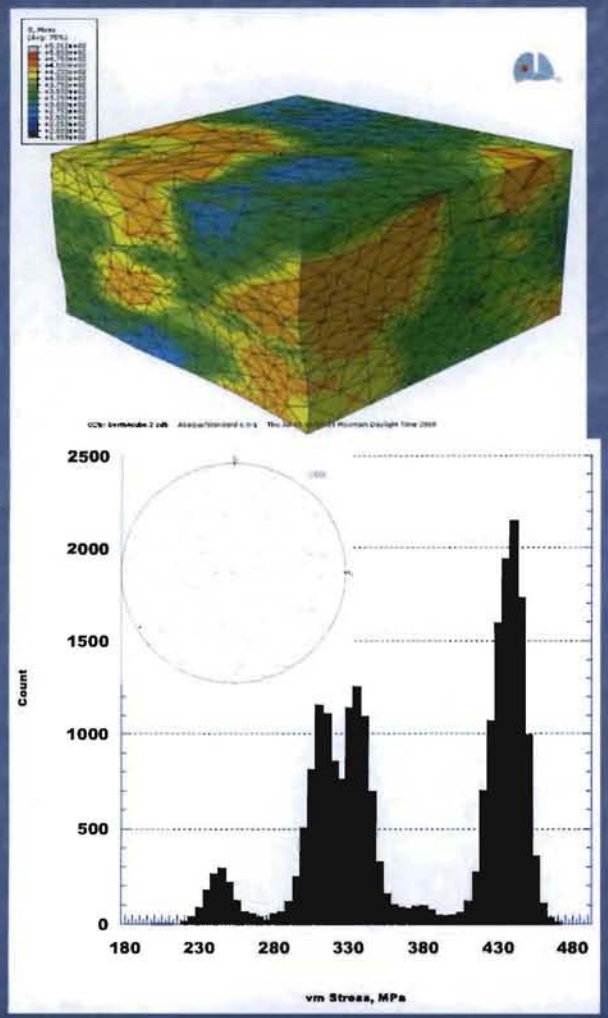

Texture 2

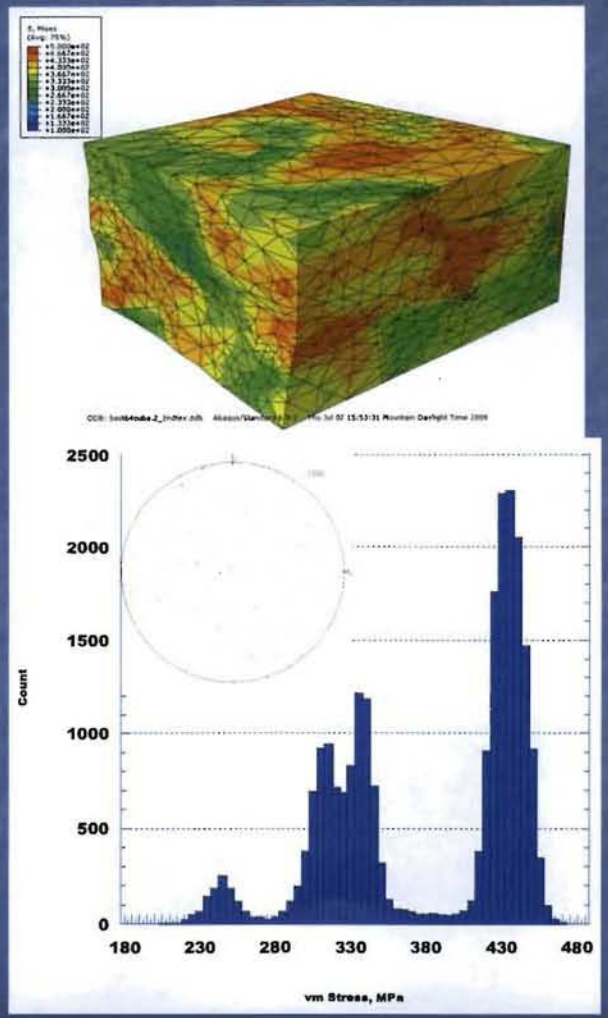

Texture 3

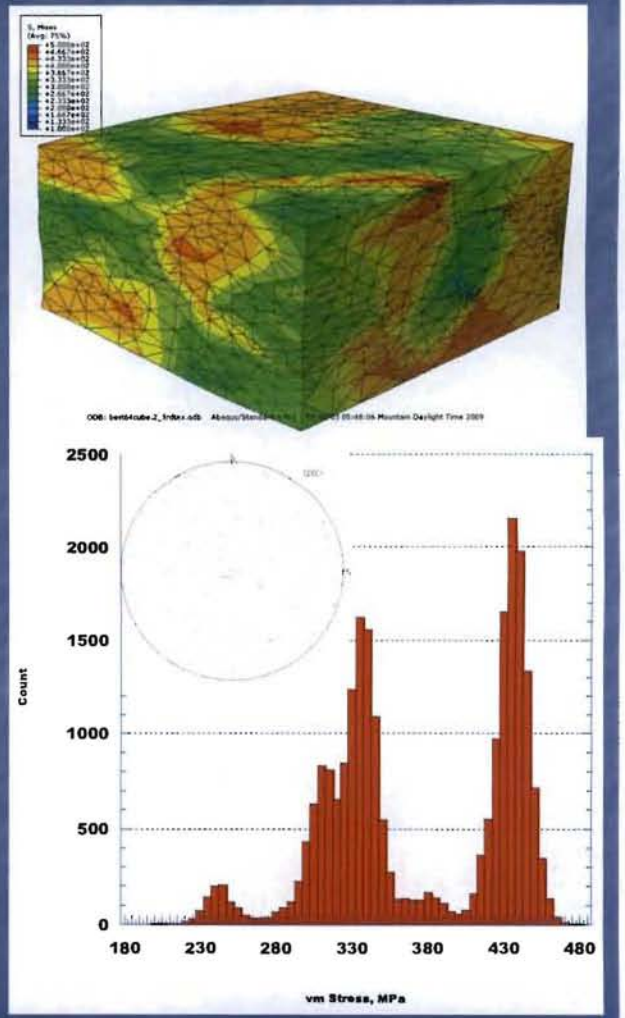

Von Mises Stress of elements.

Macroscopic Response

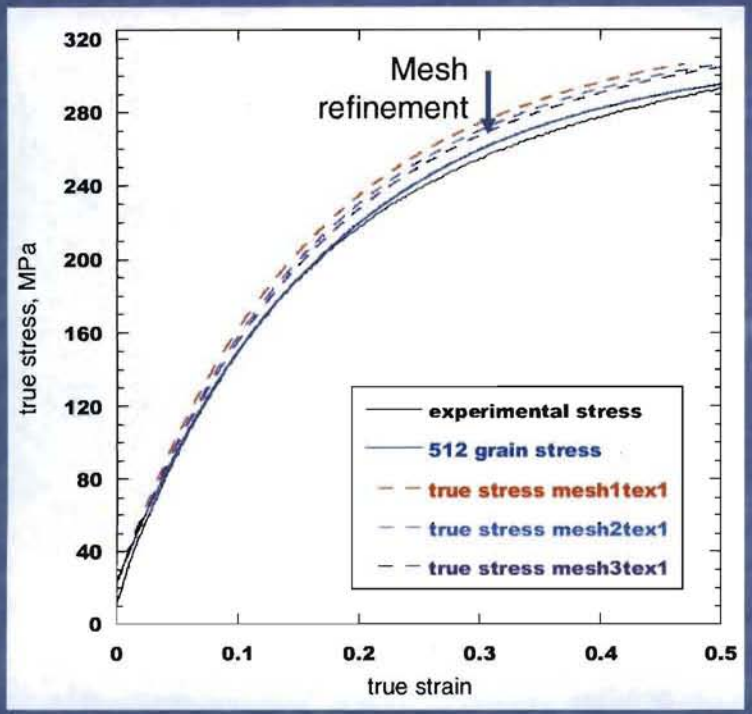

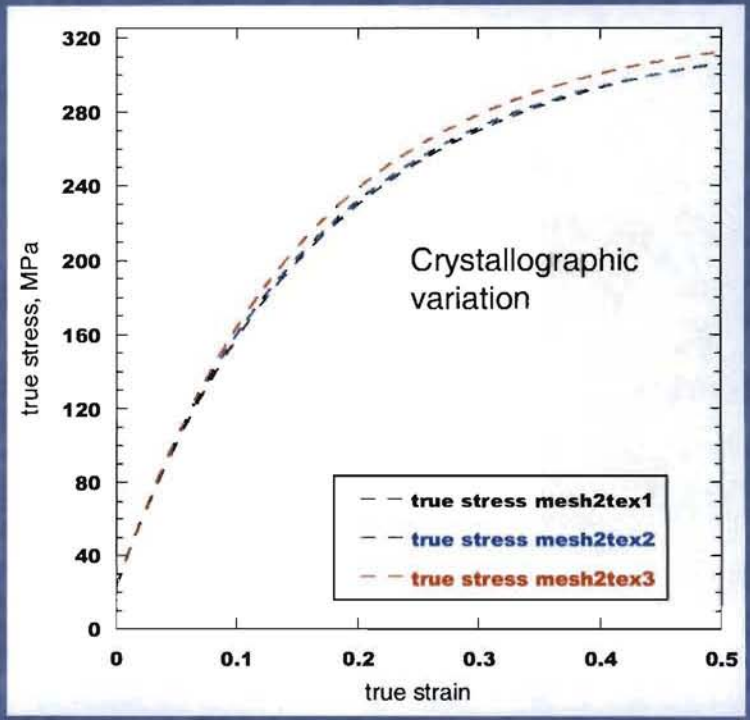

Macroscopic stress response decreases with a finer mesh size.

Crystallographic texture has a minor effect on the macroscopic stress response.

Morphologic Response

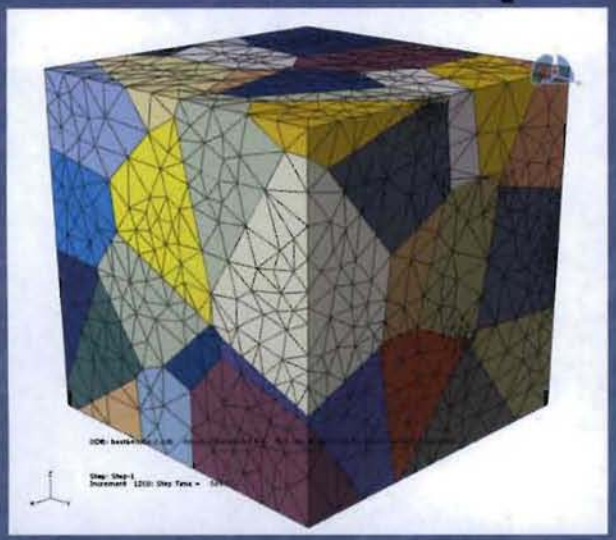

Identical 64 crystal orientations

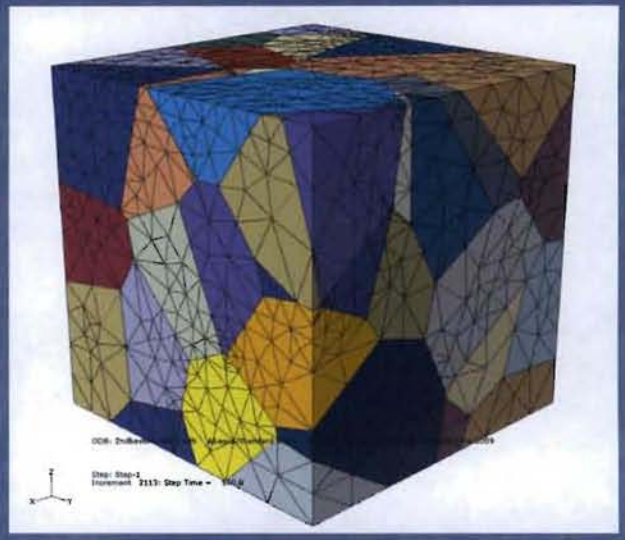

Voronoi 1

23544 Tet. Elements

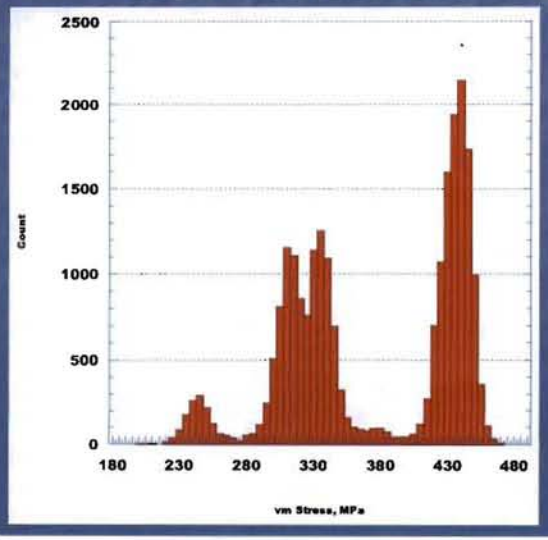

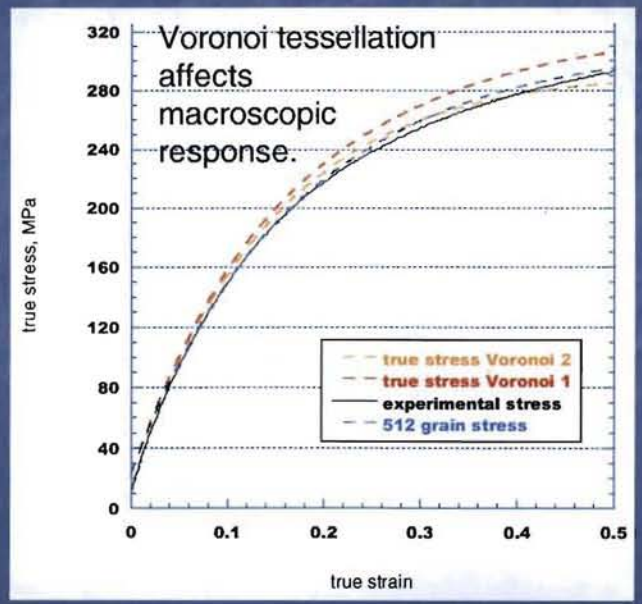

Voronoi 2

23351 Tet. Elements

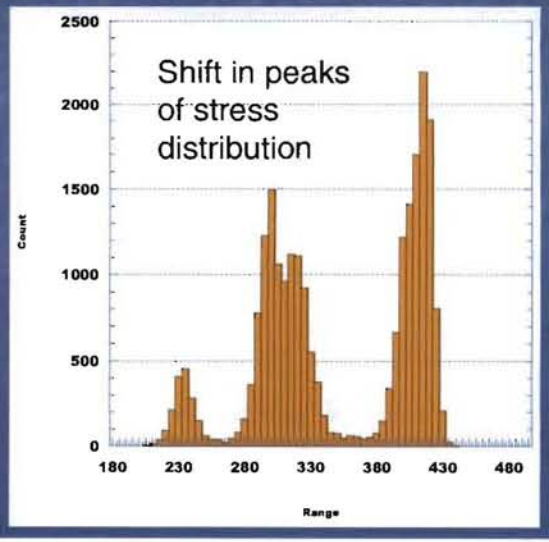

Subgrain Dislocation Structures

- Plastic deformation in metals typically involves motion of dislocations within the atomic lattice.
- Dislocation walls form by dissimilar dislocations interacting.
  - Seen at higher strain states through TEM analysis.
  - Material separates into distinct areas.
  - Act as boundaries to further dislocation motion (plastic deformation).
  - These are "geometrically necessary" boundaries, as opposed to statistical or incidental dislocation boundaries.

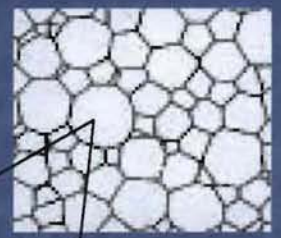

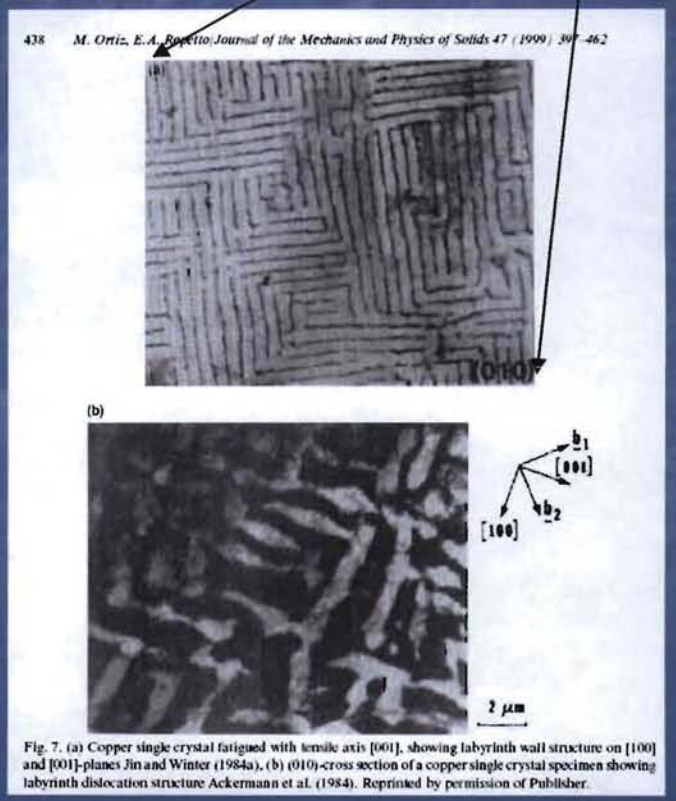

Fig. 7. (a) Copper single crystal fatigued with tensile axis [001], showing labyrinth wall structure on [100] and [001]-planes Jin and Winter (1984a). (b) (010)-cross section of a copper single crystal specimen showing labyrinth dislocation structure Ackermann et al. (1984). Reprinted by permission of Publisher.

Subgrain Laminate Microstructures

Tractable mathematically as energy minimization.

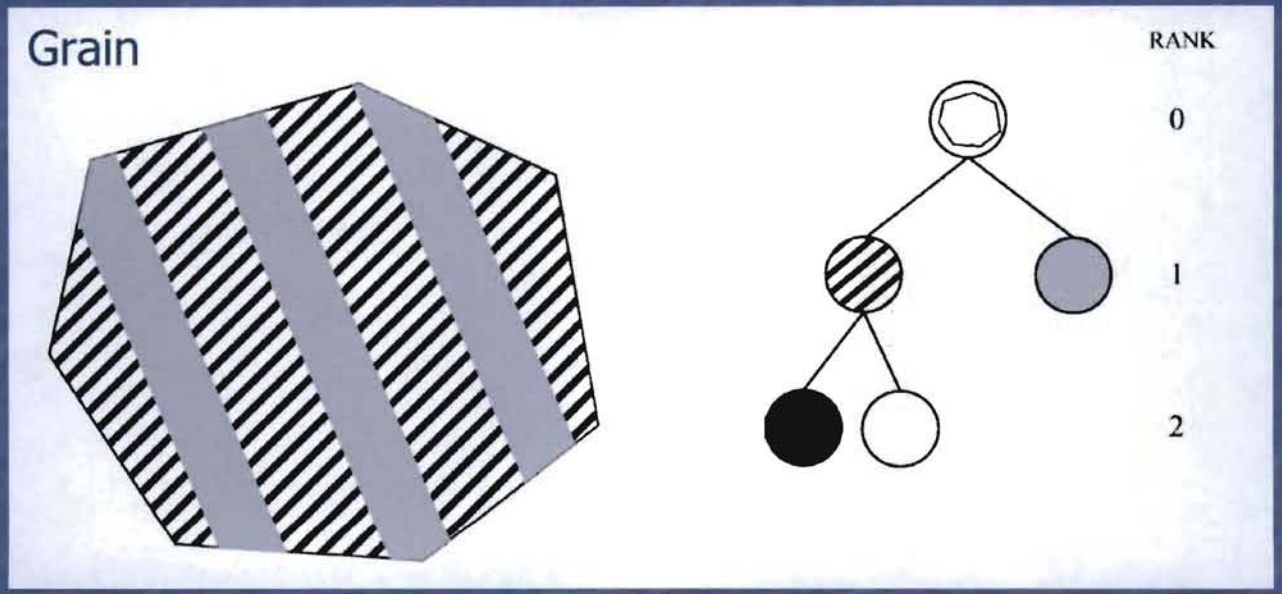

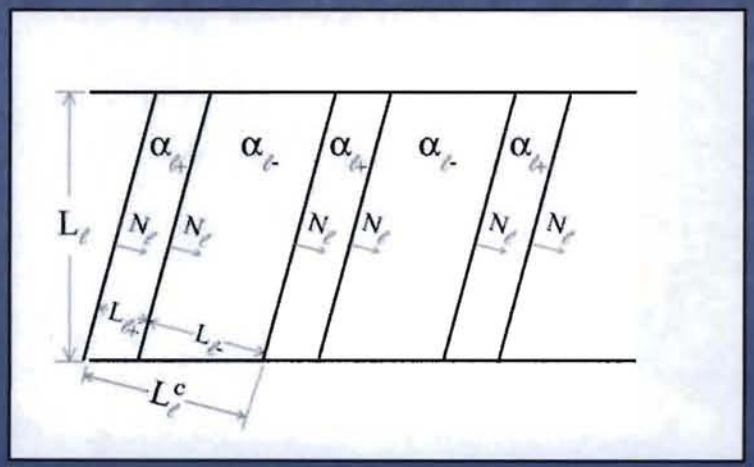

Characterized by:

a = polarization vector α = slip system

N = wall normal - coplanar

λ = volume fraction

L^c = length scale

Rank 1 connected deformations: $${}_n\mathbf{F}_{l+} - {}_n\mathbf{F}_{l-} = {}_n\mathbf{a}_l \otimes \mathbf{N}_l$$

Mean Free Path Shortening

- When dislocation walls form the mean free path of dislocations is shortened.

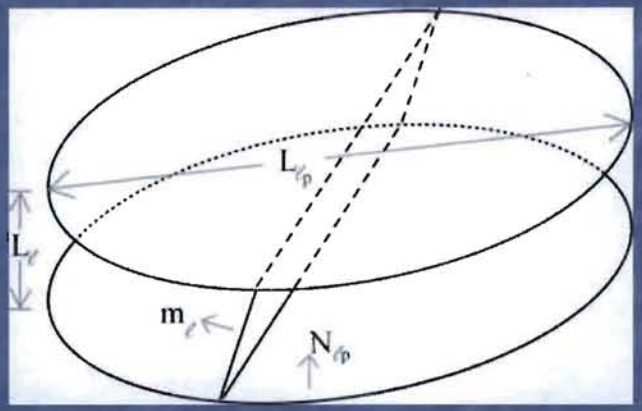

- The actual length depends on the angle between the slip plane and the dislocation wall:

$$A = \frac{L_l}{\sqrt{1-(\mathbf{m}_l \cdot \mathbf{N}_{l_p})^2}}$$
$$B = L_{l_p}$$

- Coplanar slip is a special case and must be accommodated within a single laminate.
- By Orowan's relation, shortening the mean free path, h, increases the critically resolved shear stress:

$$_n\tau_l^c = \tau_0^c + \frac{T}{b\ _n h_l}$$

Laminate Microstructures: Non-local Energy

- The non-local energy is the combination of the energy gained from the dislocation walls and the mismatch at the boundary.

$$ {}_nW_l^{NL} = {}_nW_l^{DW} + 2\Upsilon \frac{{}_nL_l^c}{{}_{n-1}L_l} {}_nW_l^{BL} $$

- The laminate thickness is determined by the minimization of the non-local energy.

$$ {}_nL_l^c = \sqrt{\frac{T\ {}_{n-1}L_l}{2\Upsilon b\ {}_nW_l^{BL}} \left(\frac{{}^n\gamma_{l-}}{\lambda_{l-}} \sqrt{1-(\mathbf{m}_{l-}\cdot\mathbf{n}_l)^2} + \frac{{}^n\gamma_{l+}}{\lambda_{l+}} \sqrt{1-(\mathbf{m}_{l+}\cdot\mathbf{n}_l)^2} \right)} $$

$$ {}_nL_l^c = \begin{cases} \textit{equation 3.24} & \textit{,if (equation 3.24)} < {}_{n-1}L_l \\ {}_{n-1}L_l & \textit{,otherwise} \end{cases} $$

Laminate Length Evolution

- To obtain correct time evolution of hardening it is essential to update the widths within the microstructure:

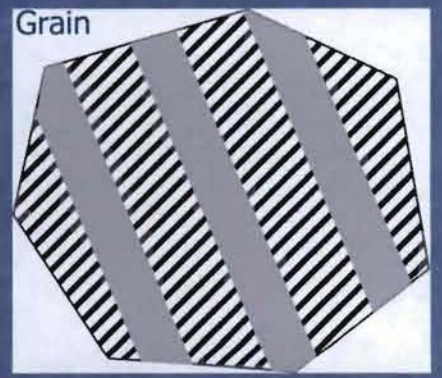

$$\min_{L_l^c,\ l=1,\ldots,Z} \sum_{l'=1}^{Z} W_{l'}^{NL}$$

$$L_l^c = \sqrt{\left(\frac{L_{l+}^c W_{l+}^{BL}}{\lambda_{l+}} + \frac{L_{l-}^c W_{l-}^{BL}}{\lambda_{l-}} + \frac{\delta_l}{2\Upsilon}\right)\frac{\lambda_l}{W_l^{BL}} L_{l_p}^c}$$

$$\delta_l \equiv \frac{T}{b\zeta}\left(\frac{\gamma_{l+}}{\lambda_{l+}}\sqrt{1-(m_{l-}\cdot N_l)^2} + \frac{\gamma_{l-}}{\lambda_{l-}}\sqrt{1-(m_{l-}\cdot N_l)^2}\right)$$

*Note both traditional mechanisms of hardening are reproduced by the laminate size evolution: self hardening and multislip hardening.

102 Structure

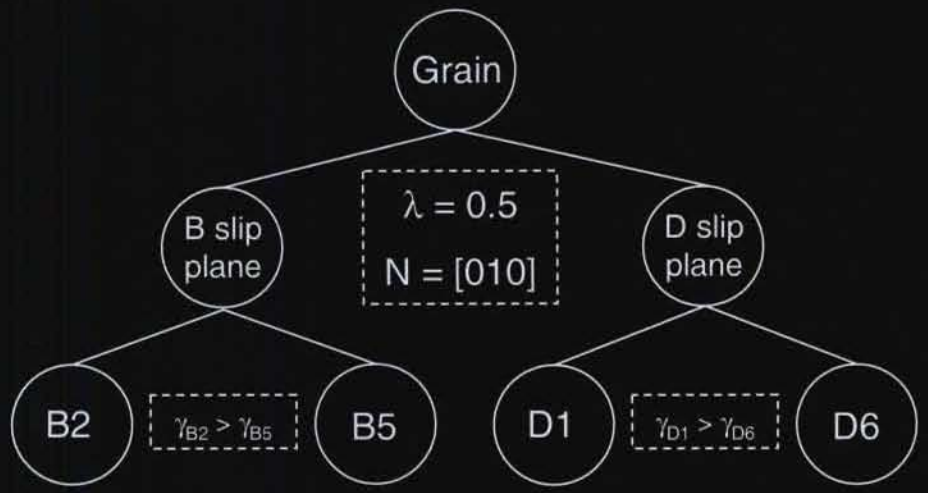

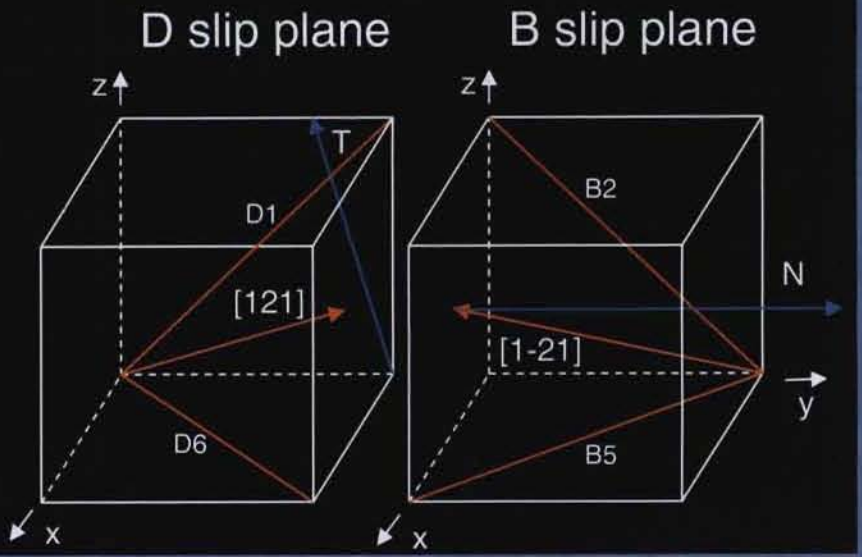

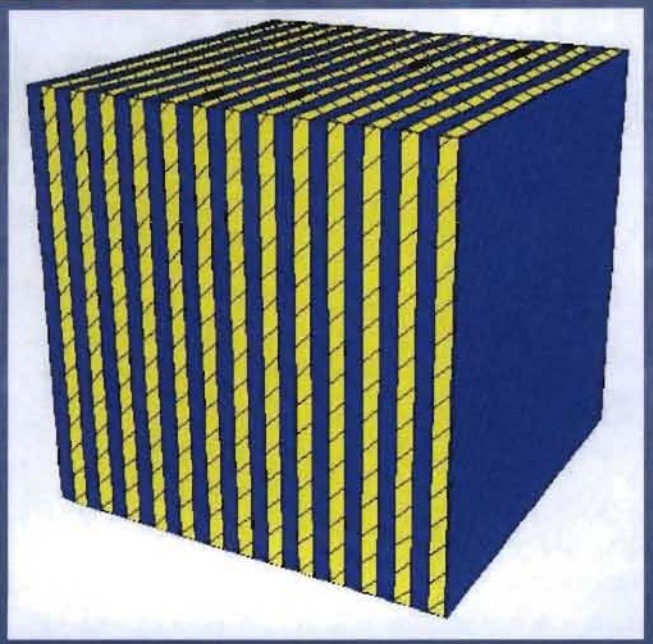

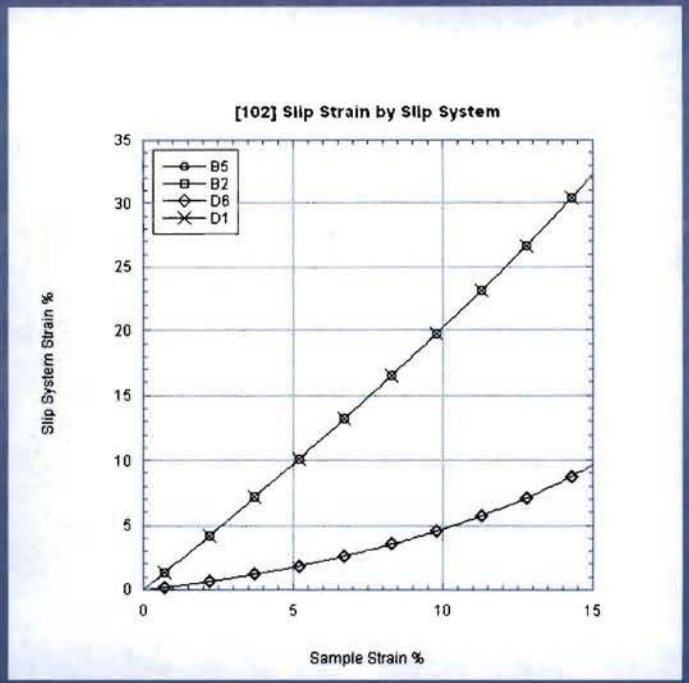

Size Dependency

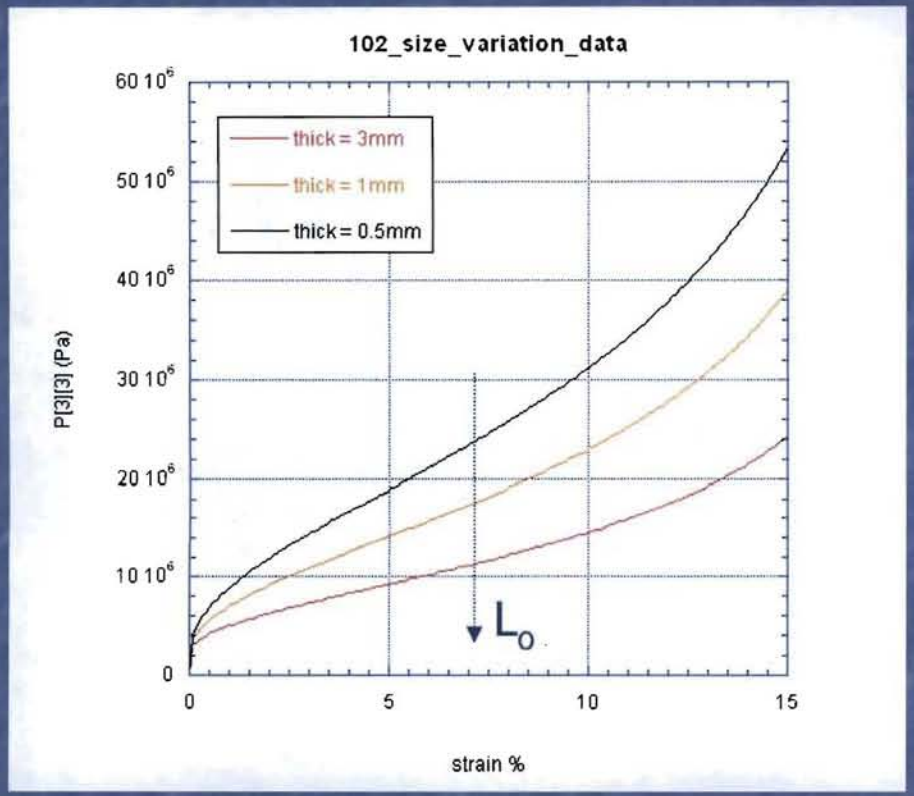

Variation in L for the 102 orientation simulations.

Relationship is Hall-Petch as predicted.

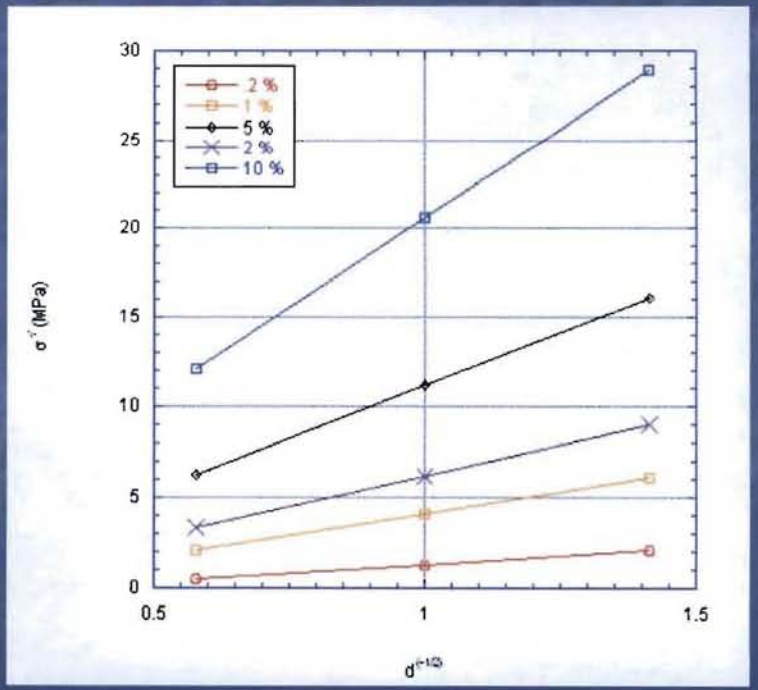

Summary

- Conclusions
  - Mesh generation is successful
  - Required mesh resolution could result in lengthy calculations
  - Crystallographic texture appears to have minor influence on macroscopic response.
  - Morphological texture has a significant impact on stress response.
- Future work
  - Include size effects in materials model
  - Further refine meshing technique
  - Analyze traction at grain boundaries
    - Against orientation
    - Against misorientation angle
    - Against grain size
  - Refine grain model – improved Voronoi or other models
  - Further comparison to experiments
  - Tri-modal distribution

Individual Grains